Systems/Circuits

Muscarinic Acetylcholine M_2 Receptors Regulate Lateral Habenula Neuron Activity and Control Cocaine Seeking Behavior

Clara I.C. Wolfe, Eun-Kyung Hwang, Elfrieda C. Ijomor, Agustin Zapata, Alexander F. Hoffman, and Carl R. Lupica

U.S. Department of Health and Human Services, National Institutes of Health, National Institute on Drug Abuse Intramural Research Program Computational and Systems Neuroscience Branch, Electrophysiology Research Section, Baltimore, MD 21224

The lateral habenula (LHb) balances reward and aversion by opposing activation of brain reward nuclei and is involved in the inhibition of responding for cocaine in a model of impulsive behavior. Previously, we reported that the suppression of cocaine seeking was prevented by LHb inactivation or nonselective antagonism of LHb mAChRs. Here, we investigate mAChR subtypes mediating the effects of endogenous acetylcholine in this model of impulsive drug seeking and define cellular mechanisms in which mAChRs alter LHb neuron activity. Using *in vitro* electrophysiology, we find that LHb neurons are depolarized or hyperpolarized by the cholinergic agonists oxotremorine-M (Oxo-M) and carbachol (CCh), and that mAChRs inhibit synaptic GABA and glutamatergic inputs to these cells similarly in male and female rats. Synaptic effects of CCh were blocked by the M_2-mAChR (M_2R) antagonist AFDX-116 and not by pirenzepine, an M_1-mAChR (M_1R) antagonist. Oxo-M-mediated depolarizing currents were also blocked by AFDX-116. Although M_2R activation inhibited excitatory and inhibitory inputs to LHb neurons, the effect on excitation was greater, suggesting a shift in excitatory-inhibitory balance toward net inhibition. Activation of VTA inhibitory inputs to LHb neurons, via channelrhodopsin-2 expression, evoked IPSCs that were inhibited by M_2Rs. Finally, we measured LHb-dependent operant response inhibition for cocaine and found it impaired by antagonism of M_2Rs, and not M_1Rs. In summary, we show that a cholinergic signal to LHb and activation of M_2Rs are critical to enable inhibition of responding for cocaine, and we define cellular mechanisms through which this may occur.

Key words: **acetylcholine; addiction; electrophysiology; impulsive behavior; muscarinic; response inhibition**

Significance Statement

The lateral habenula (LHb) is a brain region receiving information from brain areas involved in decision-making, and its output influences motivation, reward, and movement. This interface between thoughts, emotions, and actions is how the LHb permits adaptive behavior, and LHb dysfunction is implicated in psychiatric and drug use disorders. Silencing the LHb impairs control over cocaine seeking in rats, and mAChRs are also implicated. Here, we measured cocaine seeking while blocking different mAChRs and examined mechanisms of mAChR effects on LHb neurons. M_2-mAChRs were necessary for control of cocaine seeking, and these receptors altered LHb neuron activity in several ways. Our study reveals that LHb M_2-mAChRs represent a potential target for treating substance use disorders.

Received Apr. 1, 2022; revised May 12, 2022; accepted May 29, 2022.

Author contributions: C.I.C.W., E.-K.H., A.Z., A.F.H., and C.R.L. designed research; C.I.C.W., E.-K.H., E.C.I., A.Z., and A.F.H. performed research; C.I.C.W., E.-K.H., E.C.I., A.Z., A.F.H., and C.R.L. analyzed data; C.I.C.W. and A.F.H. wrote the first draft of the paper; C.I.C.W., E.-K.H., E.C.I., A.Z., A.F.H., and C.R.L. edited the paper; C.I.C.W. and C.R.L. wrote the paper.

This work was supported by the National Institutes of Health and the National Institute on Drug Abuse Intramural Research Program, Project #1ZIADA000457 to C.R.L. E.C.I. was supported by the National Institute on Drug Abuse IRP Scientific Director's Fellowship for Diversity in Research.

E.-K. Hwang's present address: Department of Behavioral Neuroscience, Oregon Health Sciences University, Portland, Oregon 97239.

The authors declare no competing financial interests.

Correspondence should be addressed to Carl R. Lupica at clupica@mail.nih.gov.

https://doi.org/10.1523/JNEUROSCI.0645-22.2022

Introduction

The lateral habenula (LHb) forms part of the habenular complex, a structure at the posterior dorsomedial end of the epithalamus (Sutherland, 1982; Kim and Chang, 2005). Early reports described the LHb as a hub collecting information from limbic forebrain inputs and relaying this to major monoaminergic nuclei (Sutherland, 1982; Christoph et al., 1986). More recently, Matsumoto and Hikosaka (2007) showed that monkey LHb neurons are activated by negative prediction errors triggered by receiving smaller than expected rewards, and are inhibited when expected positive rewards are received (Matsumoto and Hikosaka, 2007). Importantly, this LHb

neuron activity opposed that of dopamine (DA) neurons, suggesting that the LHb may counterbalance reward (Matsumoto and Hikosaka, 2007). Later studies showed that the LHb influenced DA neurons indirectly through its synaptic excitation of inhibitory neurons in the rostromedial tegmentum (RMTg) that form GABAergic synapses with DA cells (Jhou et al., 2009; Balcita-Pedicino et al., 2011; Barrot et al., 2012). Through this circuit, the LHb influences motivated behavior by processing rewarding and aversive stimuli to bias the strength and timing of DA system output (Koob and Le Moal, 2008; Stopper et al., 2014).

The LHb is also implicated in human substance use and major depressive disorders (Shabel et al., 2014; Yang et al., 2018), and it has been incorporated into opponent process theory related to reward and motivation (Solomon, 1980; Ettenberg et al., 1999). Consistent with this, drugs having rewarding properties often have delayed aversive effects that promote continued drug seeking to forestall aversion. For example, cocaine is initially rewarding followed by delayed aversion (Ettenberg et al., 1999; Lecca et al., 2017), and LHb neuron activity parallels these phases (Matsumoto and Hikosaka, 2007; Jhou et al., 2013; Neumann et al., 2014). Inactivation of LHb also disrupts reward choice bias and response inhibition for cocaine suggesting a role for the LHb in reward-based decision-making (Stopper et al., 2014) and in control of drug seeking (Zapata et al., 2017).

Most LHb neurons are glutamatergic (Brinschwitz et al., 2010; Aizawa et al., 2012), with few intrinsic GABAergic neurons identified (Webster et al., 2021). Therefore, inhibition of excitatory LHb output may be largely from extrinsic sources (Zhang et al., 2016; Wagner et al., 2017). Inhibitory LHb afferents from the lateral preoptic area (Barker et al., 2017), lateral hypothalamus (LH) (Lecca et al., 2017; Lazaridis et al., 2019), ventral pallidum (Faget et al., 2018), VTA (Stamatakis et al., 2013; Root et al., 2014a), and medial dorsal thalamus (Webster et al., 2020) have all been characterized. These afferents suppress LHb output and are generally rewarding in behavioral assays. In contrast, excitation of the LHb by lateral preoptic area (Barker et al., 2017), entopeduncular nucleus (Li et al., 2021), ventral pallidum (Faget et al., 2018), and LH (Stamatakis et al., 2016; Lazaridis et al., 2019) increase LHb output and is aversive in rodents. Additionally, some LHb inputs (e.g., VTA and entopeduncular nucleus) corelease both GABA and glutamate (Root et al., 2014b, 2018; Shabel et al., 2014).

Understanding the diversity of these afferents and their integration at the neuronal level is important for understanding the LHb's contribution to behavior. In particular, reduced inhibition increases LHb excitation, and LHb hyperactivity is implicated in depression (Shabel et al., 2014) and drug withdrawal (Shabel et al., 2014; Meye et al., 2016; Root et al., 2018). However, the influence of other regulators of LHb neuron activity on behavior is poorly understood. Notably, LHb cholinergic signaling is implicated in inhibiting cocaine seeking in a model of impulsive behavior (Zapata et al., 2017), and there is strong evidence for cholinergic innervation of the LHb from inputs, including the hindbrain pontomesencephalic tegmentum and basal forebrain cholinergic nuclei (Fibiger, 1982; Contestabile and Fonnum, 1983; Woolf and Butcher, 1986). Here, we investigated mechanisms of cholinergic control of LHb neuron activity and used a model of response inhibition to evaluate how this influences cocaine-motivated behavior.

Materials and Methods

Subjects

Male and female Long Evans rats (Charles River Laboratories) aged 4-6 weeks were housed 2-4 same sex animals per cage in an Association for Assessment and Accreditation of Laboratory Animal Care International accredited facility. They were maintained in a temperature- and humidity-controlled environment with *ad libitum* food and water. Rats used in electrophysiological experiments were housed under standard lighting conditions (lights on 6:00 A.M., off 6:00 P.M.). For behavioral experiments, rats were housed under a reverse 12 h light/dark cycle and experiments were performed during the dark phase. All animal procedures were approved by the Animal Care and Use Committee of the National Institute on Drug Abuse Intramural Research Program and conducted in accordance with the Guide for the care and use of laboratory animals (National Research Council, 2011).

Electrophysiology

Rats were anesthetized with isoflurane and decapitated using a guillotine. The brains were extracted and transferred to ice-cold HEPES-modified cutting solution (in mM as follows: 92 NaCl, 3 KCl, 1.2 NaH_2PO_4, 30 $NaHCO_3$, 20 HEPES, 25 glucose, 5 ascorbic acid, 10 $MgCl_2$, 0.5 $CaCl_2$). The tissue was blocked with a razor blade and glued to the stage of a vibrating tissue slicer (Leica VT1200S, Leica Biosystems). Coronal slices (280 μm) containing the LHb, and corresponding to ~3.3 mm to 4 mm posterior to bregma (Paxinos and Watson, 2007), were transferred to a holding chamber containing normal aCSF consisting of the following (in mM): 126 NaCl, 3.0 KCl, 1.5 $MgCl_2$, 2.4 $CaCl_2$, 1.2 NaH_2PO_4, 11.0 glucose, 26 $NaHCO_3$, saturated with 95% O_2/5% CO_2, at 35°C for 15-20 min, and then stored at room temperature. A hemisected brain slice was submerged in a recording chamber (~170 μl volume; Warner Instruments) integrated into a fixed stage of an upright microscope (Olympus BX51WI), and perfused with warm (31°C-33°C) aCSF at 2 ml/min using a peristaltic pump. The aCSF was warmed using an inline solution heater (TC-324B, Warner Instruments). Drugs were prepared as stock solutions in H_2O or DMSO and diluted in aCSF to the indicated concentrations. Visualization of LHb neurons was performed using gradient contrast microscopy with infrared illumination. Recordings were performed in the medial LHb (mLHb), a region corresponding to the parvocellular subnucleus and central subnucleus (Geisler et al., 2003). Whole-cell voltage-clamp recordings were performed using a MultiClamp 700B (Molecular Devices), WinLTP software (version 3.0, WinLTP, Ltd.), and an A/D board (PCI-6251, National Instruments). Series resistance was monitored using hyperpolarizing steps (−10 mV, 200 ms), and cells demonstrating >20% change in access resistance were excluded from analyses.

In experiments in which sIPSCs alone were recorded, electrodes (4-6 MΩ) were filled with the following (in mM): 145 KCl, 10 HEPES, 0.2 EGTA, 2 $MgCl_2$, 4 Mg-ATP, 0.3 Na_2-GTP, 10 Na_2-phosphocreatine, pH 7.2 with KOH. For experiments in which sEPSCs and sIPSCs were recorded in the same cells, or when electrically evoked (eIPSC) or light-evoked IPSCs (oIPSC) were recorded, the electrodes were filled with the following (in mM): 140 K-gluconate, 5 KCl, 10 HEPES, 0.2 EGTA, 2 $MgCl_2$, 4 Mg-ATP, 0.3 Na_2-GTP, 10 Na_2-phosphocreatine, pH 7.2 with KOH. For neurons clamped at 0 mV, QX-314 (1 mM) was added to the intracellular solution. Except when EPSCs and IPSCs were recorded in the same neurons, IPSCs were pharmacologically isolated using 6,7-dinitroquinoxaline-2,3-dione (DNQX, 10 μM), and EPSCs were isolated in the presence of picrotoxin (100 μM). In some experiments, gabazine (10 μM) or DNQX (10 μM) was bath-applied at the end of recordings to confirm the nature of the synaptic response.

Electrically evoked responses were obtained by positioning the tips of a bipolar stimulating electrode (FHC) on the surface of the brain slice 150-200 μm from the recording electrode within the LHb. Stimulation intensity was adjusted to elicit a response 30%-50% of the peak amplitude. For oIPSCs, a 473 nm diode-pumped solid state laser (OEM Laser BL-473-00200) was used to deliver a single 473 nm blue light pulse (5 ms) that was collimated through a 40× objective using a fiber optic adaptor (IS-OGP; Siskiyou). Evoked responses were obtained every 30s, and spontaneous synaptic events were collected as continuous recordings before and during drug application. Continuous

event recordings of spontaneous currents were analyzed offline in 2 min epochs collected before and during drug application. Event detection of spontaneous synaptic currents was performed using WinEDR (University of Strathclyde, Glasgow, UK), using a template-based matching algorithm (Clements and Bekkers, 1997). Typical detection parameters for sEPSCs used rise times of 0.3 ms and decay times of 3 ms, and individual events were confirmed by visual inspection. Excitatory-inhibitory (E-I) ratios were calculated by measuring eEPSCs at −70 mV (inward currents) and eIPSCs at 0 mV (outward currents) within the same cell. The stimulation intensity for these experiments was adjusted to produce an eEPSC that was ∼50% of maximum. The E-I ratio was defined as the proportion of excitatory synaptic current to the total synaptic current recorded in each cell, or E/E + I, using the area under the curve of 6-10 events averaged during the control predrug period and during drug application (Antoine et al., 2019). To analyze E-I ratios independently of electrical stimulation, we also measured sEPSCs (−70 mV holding potential) and sIPSCs (0 mV holding potential) in the same LHb neurons during 30-60 s periods under control conditions and during carbachol (CCh) or CCh + AFDX-116 application. The area of each spontaneous synaptic current (pA*ms) was calculated and all currents summed over the entire time window to obtain the total membrane charge transfer (Q). The E-I ratio was then calculated as a ratio of the total charge transfer associated with the sEPSCs and sIPSCs using the equation $[(Q_{sEPSC})/(Q_{sEPSC} + Q_{sIPSC})]$.

Surgery

Virus infusions. Rats were positioned in a stereotaxic frame (Kopf Instruments) and initially anesthetized with isoflurane (4% delivered at a flow rate of ∼1 L/min O_2) using a calibrated vaporizer. Thereafter, anesthesia was maintained with 1%-1.5% isoflurane delivered at a flow rate of ∼0.2 L/min O_2. Body temperature was maintained at 37°C with a heating pad and a sterile "tips only" technique was used for all surgeries. A 10 µl Hamilton syringe connected to an UltraMicroPump and SYS-Micro4 controller (WPI) was used to deliver 0.7 µl of AAV5-hSyn-hChR2(H134R)-eYFP (University of North Carolina vector core), over 5 min, into the medial VTA (AP: −5.4; ML: ±2.0; DV −8.2; 10° angle). After surgery, incisions were closed with absorbable sutures, and rats received an injection of the nonsteroidal anti-inflammatory meloxicam (1 mg/kg, s.c.) before being returned to their home cage where they were monitored for the next 3 d. Animals were euthanized for *in vitro* electrophysiology 6-8 weeks following virus infusion.

Self-administration and LHb cannulae implantation. Surgical anesthesia was achieved with equithesin (1% pentobarbital, 2% magnesium sulfate, 4% chloral hydrate, 42% propylene glycol, 11% ethanol, 3 ml/kg, i.p.), diluted 1:3-33% in saline immediately before injection to minimize peritonitis, and anesthetic depth was assessed throughout the procedure. Rats were then stereotaxically implanted with bilateral guide cannulae (C315, Plastics One) aimed 1 mm dorsal to the LHb (coordinates: AP: −3.8, L: ±0.6, V: −3.6 mm relative to bregma). Rats included in Go/NoGo intravenous self-administration (IVSA) studies were also implanted with a polyurethane catheter (Instech) that was inserted 3.5 cm into the right jugular vein. The catheter terminated in a Vascular Access Button (Instech), which was dorsally mounted subcutaneously. Rats received an injection of the nonsteroidal anti-inflammatory meloxicam (1 mg/kg, s.c.) following surgery. Per Animal Care and Use Committee policy, rats were monitored daily for signs of adynamic ileus, and no such signs were observed in any subjects. All animals resumed normal feeding behavior and demonstrated weight gain during a 1 week surgical recovery phase before training in the Go/NoGo task.

Go/NoGo cocaine IVSA task

Operant training took place as described in detail previously (Zapata et al., 2017). Standard rat operant chambers (Med-Associates) were used, and rats were trained to self-administer cocaine (0.75 mg/kg/infusion) for 12 sessions (2 h or 40 infusions per session) on a schedule in which each lever press on the active lever was followed by an injection of cocaine (fixed ratio 1 [FR1] schedule). Following this, rats were trained on a Go/NoGo task consisting of 2-h-long sessions of 6 × 20 min of alternating intervals of cocaine availability (Go) and nonavailability (NoGo), signaled by a house light on during cocaine availability, and house light off when cocaine infusions did not follow lever presses. During Go periods, every fifth response (FR5) was immediately followed by a cocaine infusion, whereas responding during NoGo periods had no consequence. Training progressed until stable discrimination of the Go/NoGo periods was observed (three consecutive sessions in which NoGo responses were <30% of total, 12-14 sessions). After reaching criterion, testing proceeded using a within subject design in which each rat received bilateral LHb infusions of PBS, scopolamine (50 mM), pirenzepine (PZP, 30 mM), or AFDX-116 (30 mM), dissolved in PBS with a 0.5 µl injection volume immediately before starting the Go/NoGo cocaine IVSA session.

Drugs

CCh, oxotremorine-M (Oxo-M), the M_4-mAChR-positive allosteric modulator (PAM), VU10010, and AFDX-116 were purchased from Tocris Bioscience. DNQX and picrotoxin were obtained from Hello Bio. PZP, scopolamine, and other reagents were purchased from Sigma-Aldrich. Cocaine hydrochloride was obtained through the National Institute on Drug Abuse Drug Supply Program. TTX was obtained from Alomone Laboratories.

Data analysis

Statistical analyses were conducted using the two-tailed Student's *t* test and one- or two-way repeated-measures ANOVA (Prism 9, GraphPad Software). An α value of $p < 0.05$ was considered statistically significant. The Sidak, Tukey, or Dunnett's *post hoc* tests were performed to assess between group differences.

Results

Effects of cholinergic agonists on LHb neuron membrane currents

We previously reported that the muscarinic agonist Oxo-M produced heterogeneous effects on LHb neuron somatic excitability (Zapata et al., 2017). Here, we measured the effect of the nonselective cholinergic agonist CCh (10 µM) on LHb neuron membrane currents under voltage clamp (holding potential, V_{hold} = −60 mV). Like our previous Oxo-M data, CCh reversibly evoked outward (inhibitory) currents ($n = 16$ of 88 cells from 20 rats; 18.18%; Fig. 1*A*,*B*) and inward (excitatory) currents ($n = 31$ of 88, 35.23%; Fig. 1*A*,*B*) in neurons located in the mLHb. We additionally observed biphasic currents (brief outward followed by inward currents) in 6 of 88 (7%) of neurons. The remaining 35 cells (39.77%) showed no change in I_{hold} on CCh application. The plots in Figure 1*B* show the effect of CCh on each LHb neuron tested, together with symbols indicating the mean and 95% CI for each category. Placement into the "No Change" category occurred when the change in holding current (ΔI_{hold}) was <10 pA, whereas cells in the remaining categories demonstrated ΔI_{hold} >10 pA in either the inward or outward direction. CCh-activated outward currents were associated with a large reduction in input resistance (35.6 ± 10.5% of control), whereas cells displaying inward currents demonstrated a smaller reduction in input resistance (76 ± 6.4% of control). Input resistance was unchanged in cells displaying no change in I_{hold} (93 ± 4% of control).

In a prior study using Oxo-M under identical experimental conditions, we observed inward currents in ∼50% of LHb neurons (Zapata et al., 2017). However, in the present study, CCh-evoked inward currents were observed in only 35% of cells (Fig. 1*A*,*B*). Therefore, we compared the effects of CCh (10 µM) and Oxo-M (10 µM) in the same LHb neurons to determine whether the difference might be explained by distinct pharmacological properties of these agonists ($n = 10$). We found that Oxo-M produced inward currents in LHb neurons that were insensitive to CCh and this difference in current magnitude was significant

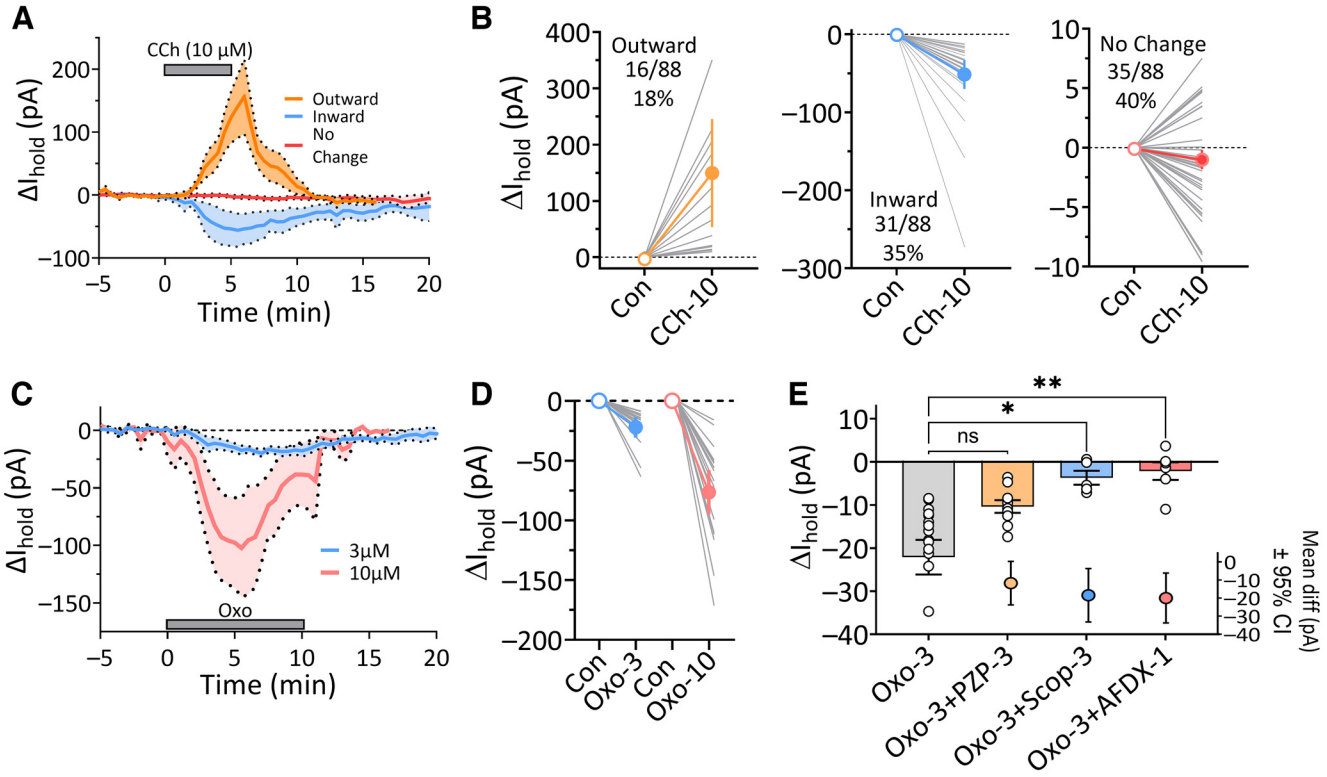

Figure 1. Effects of ACh agonists on LHb neuron excitability measured via changes in holding current (ΔI_{hold}). ***A***, Time course showing the diversity of effects of CCh (10 μM, gray bar) on I_{hold} in all recorded LHb neurons (V_{hold} = −60 mV, n = 88 cells). CCh application caused inward, outward, or no change in holding currents (mean = solid line, ± SEM = black dots and shading). ***B***, Proportions of cells demonstrating outward, inward, or no ΔI_{hold} with CCh application. Gray lines indicate changes observed in individual neurons. Symbols represent peak mean ± 95% CI ΔI_{hold}. Note the differences in y axis scales. ***C***, Time course showing the concentration-dependent effects of Oxo-M (Oxo, at 10 or 3 μM application indicated by gray bar) on I_{hold} in all recorded LHb neurons (10 μM, n = 22 cells, 3 μM, n = 16 cells, V_{hold} = −60 mV). Unlike CCh, Oxo produced inward changes in I_{hold} in most cells (89%) at either concentration. ***D***, Peak changes in I_{hold} caused by Oxo (3 and 10 μM) in all recorded LHb neurons (gray lines) and mean ± 95% CI changes for these same cells (symbols). ***E***, Effects of mAChR antagonists on inward currents caused by Oxo (3 μM). Bars represent mean (± SEM) effect of Oxo alone and, in separate groups of LHb neurons, after preincubation with the M_1-mAChR antagonist PZP (3 μM), the nonselective mAChR antagonist, scopolamine (Scop, 3 μM), or the M_2-mAChR antagonist, AFDX-116 (AFDX, 1 μM). Also shown is the mean difference 95% CI estimation plot (round symbols) of effects of 3 μM Oxo after antagonist preincubation. Both Scop and AFDX significantly reduced the effect of Oxo, whereas PZP had no significant effect (one-way ANOVA, $F_{(3,24)}$ = 10.6, p = 0.0001; p = 0.0002, Tukey's multiple comparisons, *p = 0.011, **p = 0.0029).

(−42.9 ± 11.9 pA and −7.9 ± 4.82 pA, mean ± SEM, respectively: paired t test, $t_{(9)}$ = 3.460, p = 0.0072). This suggests differences in affinity or efficacy between Oxo-M and CCh at mAChRs. Therefore, to study the pharmacology of the inward currents, we used Oxo-M at a concentration (3 μM) that yielded currents similar in amplitude to that of CCh-evoked inward currents (Fig. 1*C* vs Fig. 1*A*). The 3 μM concentration of Oxo-M produced inward currents in 16 of 18 (89%) neurons tested (2 showed no change) (Fig. 1*C*,*D*). As higher levels of expression of muscarinic M_2Rs have been reported in the LHb (Wagner et al., 2016), we next evaluated the effect of the M_2R antagonist AFDX-116 (1 μM) on Oxo-M-induced inward currents. We found that these currents were prevented by preincubation of brain slices with AFDX-116 (Fig. 1*E*; one-way ANOVA, $F_{(3,24)}$ = 10.6, p = 0.0001; p = 0.0002, Tukey's multiple comparisons), or by the nonselective antagonist scopolamine (p = 0.0013, Fig. 1*E*). In an additional group, the M_1R antagonist PZP slightly decreased the effect of Oxo-M, but this was not statistically significant (control Oxo-M inward current vs Oxo-M current in PZP, p = 0.06, Tukey's; Fig. 1*E*).

Several studies indicate that both PZP and AFDX-116 may also bind to M_4-mAChRs, which could explain this discrepancy between antagonists (Bonner, 1989; Hulme et al., 1990; Kashihara et al., 1992; Caulfield and Birdsall, 1998; Dasari and Gulledge, 2011). Therefore, we investigated whether Oxo-M-activated inward currents might involve M_4Rs by testing Oxo-M alone (3 μM), or after preincubation with the M_4R-PAM VU10010 (3 μM) (Shirey et al., 2008). We found that the effect of Oxo-M was unchanged by preincubation with VU10010 (mean and 95% CI, Oxo-M alone = −22.1 pA, −30.7 pA and −13.5 pA; Oxo-M with VU10010 preincubation = −26.47 pA, −45.8 and −7.85 pA; unpaired t test, $t_{(22)}$ = 0.55, p = 0.588, data not shown). To ensure that the concentration of VU10010 used in this experiment was sufficient to increase M_4R function, we measured its effects on the inhibition of Schaffer collateral glutamatergic field excitatory postsynaptic potentials (fEPSPs) in the CA1 region of hippocampal slices, where this has been previously demonstrated (Shirey et al., 2008). We found that the inhibition of hippocampal fEPSPs by CCh (300 nM) was significantly increased by 3 μM VU10010 (mean and 95% CI, CCh alone = −32.04%, −11.5 and −52.6%; CCh with VU10010 preincubation = −59.3%, −32.98 and −82.59%; paired t test = $t_{(4)}$ = 4.40, p = 0.012, n = 5 slices, 3 rats, data not shown). Importantly, the M_4-mediated inhibition of hippocampal fEPSPs by CCh (10 μM) was unaffected by the M_2R antagonist AFDX-116 (1 μM; mean and 95% CI, CCh alone = −81.44%, −83.76 and −79.12%; CCh + AFDX-116 = −76.65%, −81.32 and −77.98%; paired t test = $t_{(5)}$ = 1.507, p = 0.192, n = 7 slices, 4 rats, data not shown), indicating that M_4Rs were not blocked by this antagonist. Therefore, the results of our pharmacological

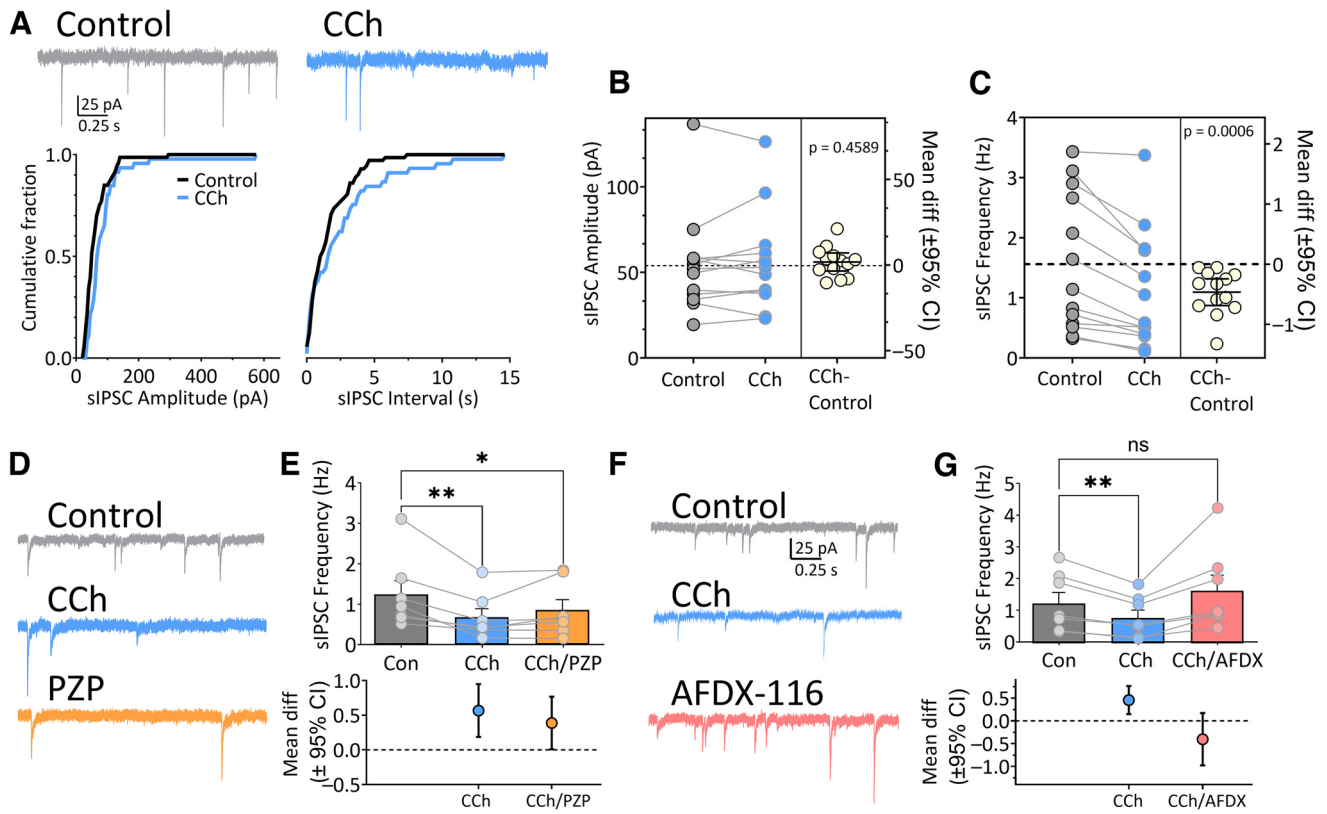

Figure 2. CCh inhibition of GABAergic transmission in LHb neurons via M_2-mAChRs. ***A***, Top, Representative traces of sIPSCs under control conditions (V_{hold} = −70 mV), and during application of CCh (10 μM). Bottom, Representative cumulative sIPSC amplitude distributions (left) and cumulative sIPSC interevent interval distributions (right) in control and CCh periods in the same cell. ***B***, Estimation plot of sIPSC amplitude for all cells under control conditions and during CCh application. The difference between control and CCh periods (CCh-control) in each cell is shown at right along with the mean difference ± 95% CI, and *p* value. CCh did not alter sIPSC amplitudes (two-tailed paired *t* test, $t_{(12)} = 0.76$, $p = 0.46$). ***C***, Estimation plot of sIPSC frequency in all LHb cells. CCh significantly inhibited sIPSC frequency (two-tailed paired *t* test, $t_{(12)} = 4.6$, $p = 0.0006$). ***D***, Representative sIPSC traces from a single LHb neuron during the control period, during CCh application, and during coapplication of CCh and the M_1-mAChR antagonist, PZP (CCh/PZP,1 μM). ***E***, Top, Group effects of CCh and CCh/PZP on sIPSC frequency in LHb neurons. PZP did not significantly reverse the effect of CCh on sIPSC frequency (one-way repeated-measures ANOVA, $F_{(2,12)} = 7.29$, $p = 0.0085$; CCh, $^{**}p = 0.005$ vs control; CCh/PZP, $^{*}p = 0.04$ vs control, Dunnett's *post hoc*). Bottom, Mean difference estimation plot of effects of CCh and CCh+PZP on sIPSC frequency for all cells. The difference between control and CCh periods and control and CCh/PZP periods is expressed as the mean difference ± 95% CI. ***F***, Representative sIPSC traces from an LHb neuron during control, CCh (10 μM) application, and during coapplication of CCh and the M_2-mAChR antagonist, AFDX-116 (CCh/AFDX, 1 μM). ***G***, Top, Group effects of CCh and CCh/AFDX on sIPSC frequency in LHb neurons. AFDX-116 significantly reversed the effect of CCh on sIPSC frequency (one-way repeated-measures ANOVA, $F_{(2,12)} = 8.71$, $p = 0.005$; CCh, $^{**}p = 0.009$ vs control; CCh/AFDX, $p = 0.15$ vs control Dunnett's *post hoc*). Bottom, Mean difference estimation plot of effects of CCh and CCh/AFDX on sIPSC frequency. The difference between control and CCh periods and control and CCh/AFDX periods is expressed as the mean difference ± 95% CI.

analysis indicate that Oxo-M-activated inward currents in LHb neurons were likely mediated by M_2Rs, and not by M_1Rs or M_4Rs.

The small number of CCh-evoked outward and biphasic currents limited our ability to study the receptors involved in these responses. However, we did find that PZP did not reverse outward currents in 6 cells (not shown).

CCh inhibits GABAergic synaptic input to LHb neurons via M_2Rs

To determine whether mAChRs also control synaptic integration in the LHb, we measured the effects of CCh on spontaneously occurring GABAergic IPSCs. Bath application of CCh (10 μM) significantly reduced the frequency of sIPSCs (Fig. 2*A*,*C*; $n = 13$ cells from 4 rats, two-tailed paired *t* test, $t_{(12)} = 4.6$, $p = 0.0006$) but had no effect on the mean amplitudes of these events (Fig. 2*B*; two-tailed paired *t* test, $t_{(12)} = 0.76$, $p = 0.46$). This effect of CCh on sIPSC frequency was not reversed by PZP (1 μM) (Fig. 2*D*,*E*; $n = 7$ cells from 4 rats; one-way repeated-measures ANOVA, $F_{(2,12)} = 7.29$, $p = 0.0085$; CCh, $p = 0.005$ vs control; CCh + PZP, $p = 0.04$ vs control, Dunnett's *post hoc*). However, AFDX-116 reversed the reduction in sIPSC frequency caused by CCh (Fig. 2*F*,*G*; one-way repeated-measures ANOVA, $F_{(2,12)} = 8.71$, $p = 0.005$; AFDX-116, $p = 0.15$ vs control, Dunnett's *post hoc*). IPSCs evoked by local electrical stimulation (eIPSCs) of the brain slice were also significantly inhibited by CCh (Fig. 3*A*,*B*; one-way repeated-measures ANOVA, $F_{(2,18)} = 13.22$, $p = 0.003$; $p = 0.002$ vs control, Dunnett's *post hoc*), and this was reversed by AFDX-116 as well ($p = 0.24$ vs control, Dunnett's *post hoc*). The effects of CCh on eIPSCs did not differ by sex (males, $n = 9$, 44 ± 6% inhibition; females, $n = 5$, 31 ± 7% inhibition; two-tailed *t* test, $t_{(12)} = 1.4$, $p = 0.18$). These data suggest that GABAergic inputs to LHb neurons are equally inhibited by presynaptic M_2Rs in male and female rats.

Inhibition of synaptic GABAergic VTA inputs to LHb by M_2Rs

As noted above, the LHb contains relatively few intrinsic sources of GABAergic inhibition (Brinschwitz et al., 2010; Aizawa et al., 2012; Wagner et al., 2017). Therefore, control of LHb neuron excitation likely arises from a diverse array of inhibitory afferents, including those from the VTA (Root et al., 2014b). As VTA neurons respond to both rewarding and aversive stimuli (Root et al., 2020) and express M_2R mRNA (Vilaro et al., 1992b), we hypothesized that this pathway would be sensitive to M_2R-

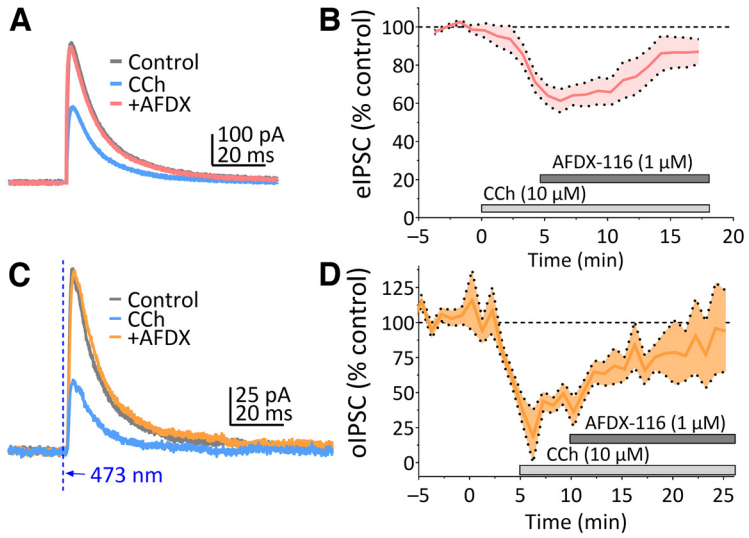

Figure 3. CCh inhibits evoked IPSCs through M_2Rs in LHb. ***A***, Representative traces of eIPSCs (V_{hold} = −45 mV, K-Gluconate intracellular solution) showing inhibition during CCh application (10 μM) and reversal by coapplication of the M_2R antagonist AFDX-116 (1 μM). ***B***, Mean (± SEM) time course showing the effects of CCh and AFDX-116 on eIPSCs in LHb neurons (n = 10 cells from 6 rats). Significant inhibition was observed following CCh (one-way repeated-measures ANOVA, $F_{(2,18)}$ = 13.22, p = 0.003; p = 0.002 vs control, Dunnett's *post hoc*), and this was reversed by AFDX-116 (p = 0.24 vs control, Dunnett's *post hoc*). ***C***, Representative traces of light-evoked oIPSCs recorded from an LHb neuron following infusion of synapsin-driven ChR2 into the VTA. Dashed line indicates the onset of a single, 5 ms duration light pulse (473 nm). ***D***, Mean time course of the effects of CCh and AFDX-116 on VTA to LHb oIPSCs (n = 5 cells from 2 rats). Significant inhibition was observed during CCh (one-way repeated-measures ANOVA, $F_{(2,8)}$ = 16.6, p = 0.001; p = 0.008 vs control, Dunnett's *post hoc*), and this was reversed by AFDX-116 (p = 0.09 vs control, Dunnett's *post hoc*).

mediated synaptic control. Rats (n = 5) received VTA injections with AAV encoding for the channelrhodopsin-2 (ChR2) protein, driven by a synapsin promoter (pAAV-hSyn-hChR2 (H134R)-EYFP), and light-evoked oIPSCs were recorded in LHb neurons 6-8 weeks later. The oIPSCs evoked by activation of ChR2 in VTA neuron axon terminals in the LHb were significantly inhibited by CCh (10 μM; Fig. 3*C*,*D*), and this was reversed by coapplication of AFDX-116 (one-way repeated-measures ANOVA, $F_{(2,8)}$ = 16.6, p = 0.001; CCh, p = 0.008 vs control; CCh + AFDX, p = 0.09 vs control, Dunnett's *post hoc*). These data suggest that VTA GABAergic inputs to LHb neurons are inhibited by M_2R activation.

CCh inhibits glutamatergic synaptic input to LHb neurons via M_2Rs

We next examined whether synaptic glutamate input to LHb neurons is modulated by mAChRs by recording sEPSCs. Unlike sIPSCs, CCh (10 μM) significantly decreased sEPSC amplitude (Fig. 4*A*,*C*–*E*; p = 0.0002, $t_{(31)}$ = 4.3, two-tailed paired t test), as well as sEPSC frequency (Fig. 4*B*,*F*; p = 0.0002, $t_{(31)}$ = 4.3, two-tailed paired t test; n = 32 neurons from 18 animals), and this was independent of sex (two-way ANOVA; sex × treatment interaction, $F_{(1,32)}$ = 0.3023, p = 0.58). Given that CCh hyperpolarizes some LHb neurons (Fig. 1), the reduction in sEPSC amplitude could reflect decreased somatic excitability of local glutamatergic LHb neurons that provide synaptic inputs to other LHb cells (Kim and Chang, 2005), as described for μ-opioids in the LHb (Margolis and Fields, 2016). Therefore, to limit the influence of somatic excitability changes on glutamate release, we measured CCh effects on mEPSCs following blockade of action potentials by CCh (200 nM). In the presence of TTX, CCh reduced mEPSC frequency (n = 9 cells from 3 rats; control, 3.3 ± 0.39 Hz; TTX, 1.9 ± 0.23 Hz; Fig. 4*H*; two-tailed paired t test, $t_{(10)}$ = 5.36, p = 0.003) but had no effect on mEPSC amplitude (control, 25.6 ± 4.1 pA; TTX, 24.9 ± 5.4 pA; Fig. 4*G*; two-tailed paired t test, $t_{(10)}$ = 0.51, p = 0.62). Additionally, noncumulative amplitude histograms indicated that CCh eliminated larger sEPSCs but also strongly reduced sEPSCs across the full range of amplitudes (Fig. 4*D*). These results suggest that CCh can reduce synaptic glutamate release onto LHb neurons via changes in somatic excitability of local presynaptic neurons, as well as by direct inhibition via effects at axon terminals.

Whereas PZP (1 μM) did not affect the inhibition of sEPSC frequency by CCh (Fig. 5*A*–*E*; one-way repeated-measures ANOVA, $F_{(2,12)}$ = 6.396, p = 0.01; $^{**}p <$ 0.01, Dunnett's *post hoc*), AFDX-116 (1 μM) reversed the CCh-mediated inhibition of sEPSC amplitude and frequency (Fig. 5*F*–*J*; one-way repeated-measures ANOVA, $F_{(2,14)}$ = 4.48, p = 0.03; CCh, p = 0.02 vs control; CCh + AFDX, p = 0.6 vs control, Dunnett's *post hoc*; one-way repeated-measures ANOVA, $F_{(2,14)}$ = 8.23, p = 0.005; CCh, p = 0.003 vs control; CCh + AFDX, p = 0.15 vs control, Dunnett's *post hoc*). Thus, M_2Rs, and not M_1Rs, inhibit synaptic glutamate release onto LHb neurons.

M_2Rs alter the excitatory-inhibitory balance of the LHb

The preceding data indicate that both excitatory and inhibitory synaptic inputs to LHb neurons are inhibited by M_2Rs. As an altered E-I balance in the LHb has been associated with a net change in neuronal activity and with dysfunctional reward valence attribution (Shabel et al., 2014; Meye et al., 2016; Mori et al., 2019), we next determined the effect of M_2R activation on LHb E-I balance (Antoine et al., 2019). CCh significantly reduced the E-I ratio measured using eEPSCs and eIPSCs in the same LHb neurons (Fig. 6*A*,*B*; n = 15 neurons from 7 animals; paired t test, $t_{(14)}$ = 2.641, p =0.0194). This change in the E-I ratio was also prevented by pretreatment with AFDX-116 (1 μM; 13 neurons from 6 animals; paired t test, $t_{(12)}$ = 0.1294, p = 0.899).

As measurement of E-I balance can be affected by differing relative degrees of sensitivity to electrical stimulation, we also measured E-I balance using sEPSCs (−70 mV holding potential) and sIPSCs (0 mV holding potential) in the same LHb neurons under control conditions and during CCh or CCh + AFDX-116 application (Fig. 6*E*–*H*). Similar to results with electrically evoked synaptic currents, we found that the E-I ratio of the spontaneous currents was significantly reduced by CCh (Fig. 6*E*,*F*; $t_{(13)}$ = 2.643, p = 0.0203, paired t test), and that this was prevented by preincubation of brain slices in 1 μM AFDX-116 (Fig. 6*G*,*H*; $t_{(12)}$ = 0.0014, p = 0.993, paired t test). Thus, whereas both excitatory and inhibitory inputs to LHb neurons using these two methods are reduced by M_2-mAChR activation, excitatory synaptic inputs are more strongly inhibited, thereby resulting in a net shift in E-I balance toward synaptic inhibition of LHb neurons.

Intra-LHb blockade of M_2Rs promotes impulsive cocaine-seeking

We previously reported that blockade of LHb mAChRs by the nonselective antagonist scopolamine impaired operant

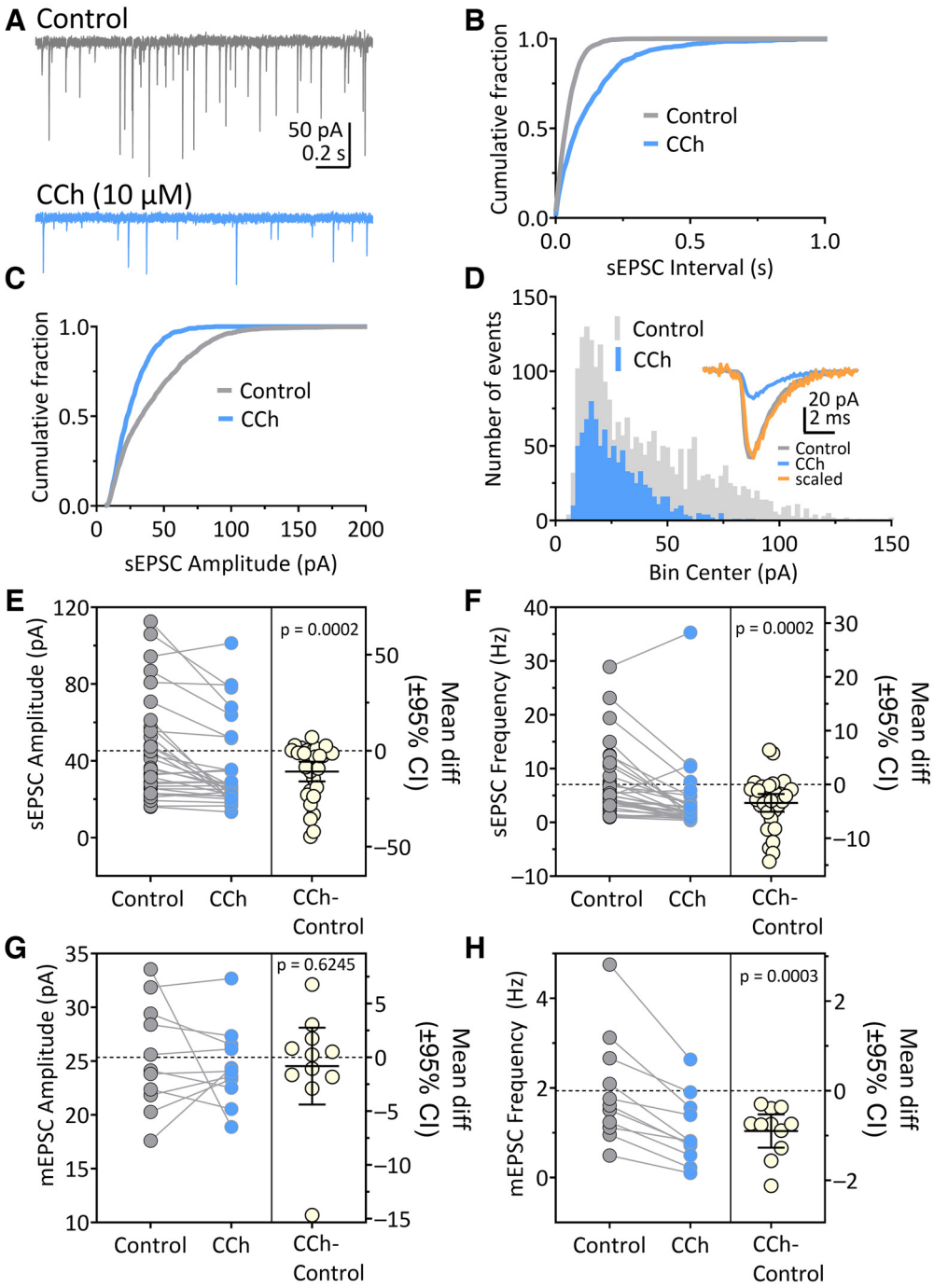

Figure 4. CCh inhibits synaptic glutamate release onto LHb neurons. ***A***, Representative sEPSC traces before and during bath application of CCh (10 μM). ***B***, Representative cumulative distribution histograms of inter-sEPSC interval and (***C***) amplitude from the same cell shows a reduction in both measures by CCh. ***D***, A noncumulative amplitude histogram from this cell shows that CCh eliminated large sEPSCs and reduced the number of sEPSCs across the full range of amplitudes. Inset, Averaged sEPSCs before and during CCh, as well as the CCh waveform scaled to the peak of the control. No change in sEPSC kinetics was observed. ***E***, Changes in mean sEPSC amplitude for all cells (left, *y* axis) and estimation plot of the mean difference ± 95% CI in this measure (CCh-control) from control to CCh periods (right, *y* axis). CCh caused a significant reduction in sEPSC amplitude (two-tailed paired *t* test, $t_{(31)} = 4.3$, $p = 0.0002$). ***F***, Estimation plot of sEPSC frequency for each LHb neuron. A significant reduction in sEPSC frequency was observed following CCh application (two-tailed paired *t* test, $p = 0.0002$, $t_{(31)} = 4.3$, $p = 0.0002$). ***G***, The amplitude of TTX-resistant (200 nM) action potential-independent mEPSCs was not significantly altered by CCh (two-tailed paired *t* test, $t_{(10)} = 0.51$, $p = 0.62$). ***H***, mEPSC frequency measured in TTX was significantly reduced by CCh (two-tailed paired *t* test, $t_{(10)} = 5.36$, $p = 0.003$). This indicates that CCh reduces sEPSC amplitude by decreasing action potential-dependent glutamate release but also inhibits TTX-resistant release.

response inhibition for cocaine in rats trained on a Go/NoGo task (Zapata et al., 2017). This suggests that intact mAChR signaling is necessary to inhibit cocaine seeking in this task. Moreover, our present electrophysiological results show that M_2Rs can alter LHb neuron membrane potential and synaptic integration in these cells. Therefore, we next asked whether M_2Rs were involved in inhibition of cocaine seeking by comparing the effects of PZP and AFDX-116 in the Go/NoGo paradigm. Rats trained to self-administer cocaine and to withhold responding during signaled drug absence received bilateral infusions of vehicle, scopolamine (50 mM), PZP (30 mM), or AFDX-116 (30 mM) before test

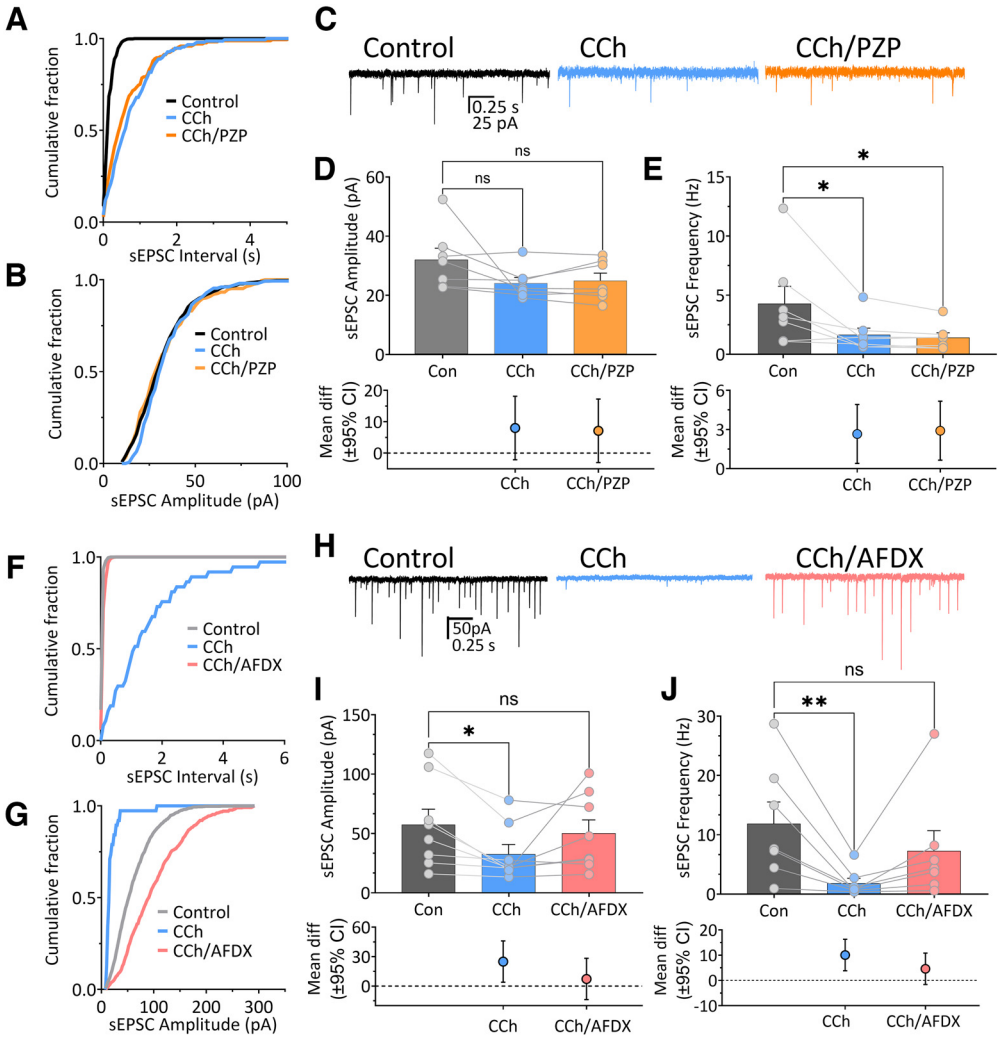

Figure 5. CCh inhibits glutamate release via M_2-mAChRs in the LHb. ***A***, Cumulative sEPSC interval and amplitude (***B***) distributions from an LHb neuron showing the effect of CCh (10 μM) and PZP (1 μM) added during CCh application. CCh did not alter the amplitude distribution in this neuron but clearly increased the sEPSC interval. ***C***, Representative sEPSC traces from the same cell represented in ***A*** and ***B***. ***D***, Mean sEPSC amplitudes for each cell under each condition are shown along with the mean differences (±95% CI) in treatment versus control. Neither CCh nor PZP significantly altered sEPSC amplitude (one-way repeated-measures ANOVA, $F_{(2,12)} = 2.351$, $p = 0.14$). ***E***, Effect of CCh and PZP on sEPSC frequency. sEPSC frequency was significantly reduced by CCh, but this was not reversed by PZP (one-way repeated-measures ANOVA, $F_{(2,12)} = 6.396$, $p = 0.01$; $^*p < 0.01$, Dunnett's *post hoc* vs control). ***F***, Cumulative distribution of sEPSC amplitude and sEPSC interval (***G***). Note the reversal of the effect of CCh by AFDX application. ***H***, Representative sEPSC traces obtained under control conditions and during successive application of CCh and AFDX-116 (AFDX, 1 μM). ***I***, Mean sEPSC amplitudes for each cell. The mean amplitude was significantly reduced (one-way repeated-measures ANOVA, $F_{(2,14)} = 4.48$, $p = 0.03$; $^*p = 0.02$ vs control, Dunnett's *post hoc*), and this was reversed by AFDX ($p = 0.6$, Dunnett's *post hoc*). The mean difference (from control) and 95% CI are shown below. ***J***, sEPSC frequency was significantly reduced by CCh (one-way repeated-measures ANOVA, $F_{(2,14)} = 8.23$, $p = 0.005$; $^{**}p = 0.003$ vs control, Dunnett's *post hoc*), and this was reversed by AFDX ($p = 0.15$ vs control, Dunnett's *post hoc*).

sessions. Whereas none of these antagonists significantly altered cocaine seeking during Go intervals (Fig. 7*A–C*; two-way repeated-measures ANOVA, Go/NoGo vs scopolamine; $F_{(1,8)} = 8.264$, $p = 0.02$; scopolamine-Go, $p = 0.71$, Sidak's; Go/NoGo vs AFDX; $F_{(1,8)} = 8.406$, $p = 0.02$; AFDX-Go, $p = 0.99$, Sidak's; two-way repeated-measures ANOVA, Go/NoGo vs PZP; $F_{(1,8)} = 0.3536$, $p = 0.57$; PZP-GO, $p = 0.99$, Sidak's), infusion of either scopolamine or AFDX-116 significantly increased responding for cocaine during NoGo periods (Fig. 7*A*,*B*, two-way repeated-measures ANOVA, drug × Go/NoGo period interaction, $p = 0.0207$ and $p = 0.0199$, respectively, Sidak's). In contrast, PZP did not significantly alter response inhibition for cocaine during NoGo periods (Fig. 7*C*; two-way repeated-measures ANOVA, Go-NoGo × drug interaction, $F_{(1,8)} = 0.3536$, $p = 0.569$). These data show that M_2Rs are critical for response inhibition in this Go/NoGo task.

Discussion

Here we describe robust modulation of neurons in the parvocellular and central subnuclei of the mLHb by mAChRs and show that the central cholinergic system, acting through M_2Rs, is critical for the withholding of operant responding for cocaine. We also find that synaptic GABA and glutamate inputs to LHb neurons are inhibited by M_2Rs, and with optogenetics we demonstrate that VTA to LHb afferents represent at least one M_2R-sensitive inhibitory synaptic pathway. Although we demonstrate that M_2Rs can inhibit both glutamate and GABA release onto LHb neurons, we also find that the net effect of M_2R activation was to bias the E-I ratio of the LHb toward enhanced inhibition. Based on this, we predict that M_2R activation will reduce excitatory LHb output to downstream targets.

In addition to the altered synaptic integration by M_2Rs, we found that mAChRs depolarize LHb neurons via activation of these receptors. Consistent with these physiological effects of

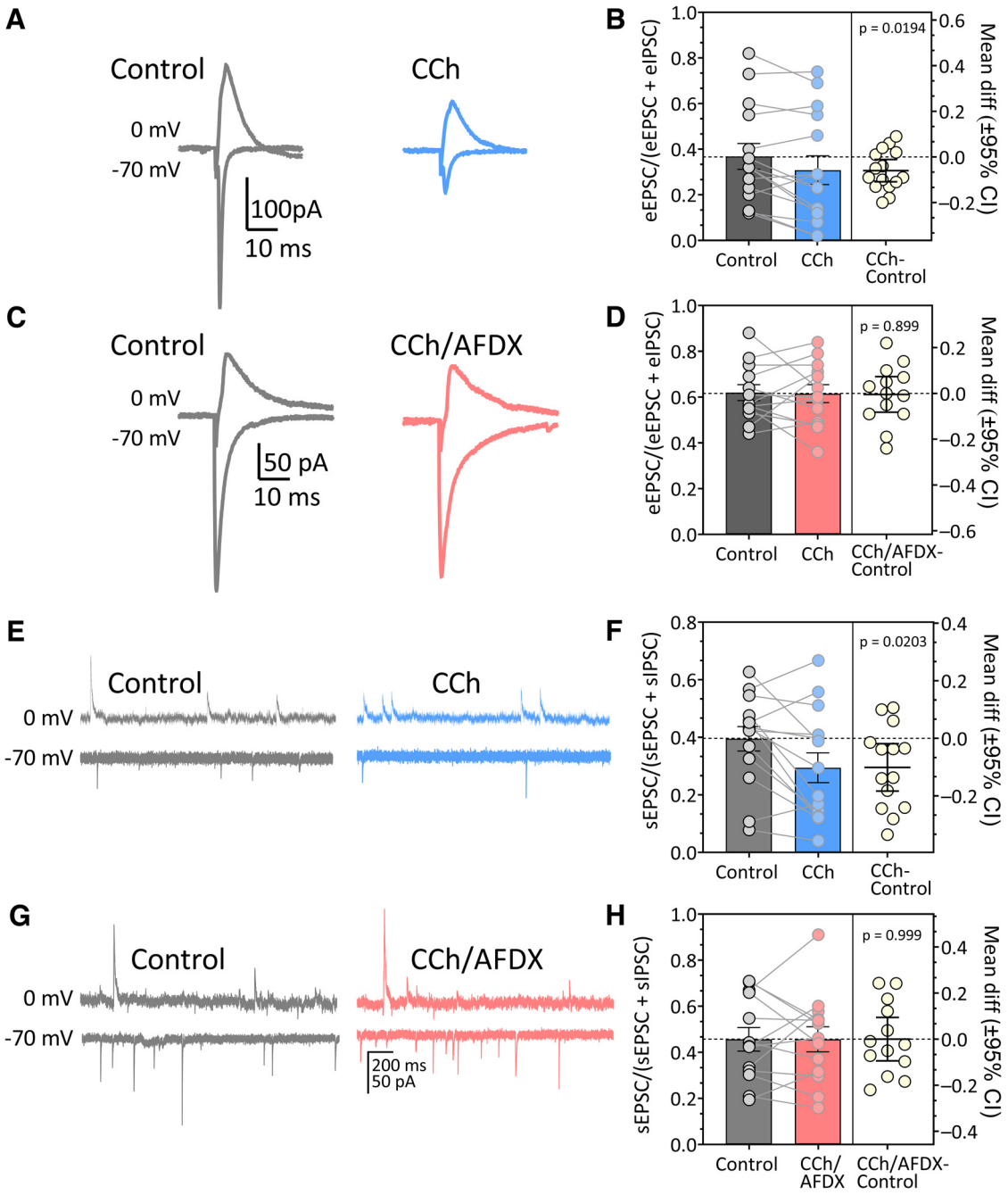

Figure 6. CCh reduces the LHb E-I balance via activation of M_2R-mAChRs. ***A***, Signal averages of eEPSCs (inward currents, downward) obtained at −70 mV, and eIPSCs (outward currents, upward) obtained at 0 mV in the same cell using the same electrical stimulus intensity. Traces were obtained before (control, gray) and during CCh (10 μM) application (blue traces). ***B***, E-I ratios for each LHb neuron in control and CCh conditions superimposed on mean E-I ratios (± SEM, bars). Right, Estimation plot showing the difference in E-I ratio for each cell obtained by subtracting the control E-I ratio from the CCh E-I ratio (CCh-Control). Also shown is the mean ± 95% CI of these differences. CCh significantly decreased the E-I ratio ($t_{(14)} = 2.641$, df = 14, $p = .0194$, paired *t* test). ***C***, eIPSC and eEPSC currents obtained during control conditions (gray traces) and during CCh application (red traces) in cells preincubated with the M_2R antagonist AFDX-116 (1 μM). ***D***, Control and CCh E-I ratios for each AFDX-pretreated LHb neuron superimposed on mean E-I ratios (± SEM, bars). Right, Estimation plot showing the difference in E-I ratio for each cell obtained by subtracting control E-I ratio from CCh/AFDX E-I ratio (CCh/AFDX-Control), and the mean ± 95% CI of these differences. CCh did not significantly change the E-I ratio in cells treated with AFDX ($t_{(12)} = 0.1294$, $p = 0.899$, paired *t* test). ***E***, sIPSC sweeps obtained at 0 mV holding potential (top) and sEPSCs obtained at −70 mV (bottom) from the same LHb cell before (Control) and during CCh application (10 μM). ***F***, E-I ratios obtained from the sIPSCs and sEPSCs in each cell before and during CCh treatment superimposed on the mean ± SEM E-I ratios (bars). Right, Estimation plot of these E-I ratio differences for each cell (CCh-Control), and the mean ± 95% CI of this difference. CCh significantly reduced the E-I ratio ($t_{(13)} = 2.643$, $p = 0.0203$, paired *t* test). ***G***, Examples of sIPSCs obtained at 0 mV holding potential (top) and sEPSCs obtained at −70 mV (bottom) from the same LHb cell preincubated with AFDX (1 μM). ***H***, E-I ratios obtained from sIPSCs and sEPSCs in each cell before and during CCh treatment in cells preincubated with AFDX (1 μM). This is superimposed on the mean ± SEM E-I ratios (bars). Right, Estimation plot of the differences in these E-I ratios in each cell during control and CCh/AFDX periods (CCh/AFDX-Control), and the mean ± 95% CI of these differences. CCh did not significantly change the E-I ratio in AFDX preincubated cells ($t_{(12)} = 0.001432$, $p = 0.993$, paired *t* test).

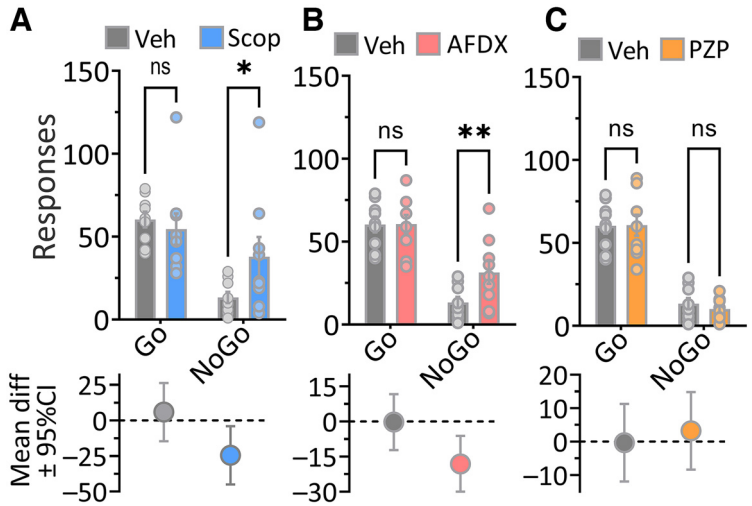

Figure 7. Blockade of LHb M_2-mAChRs impairs inhibition of responses for cocaine in a Go/NoGo cocaine self-administration task. ***A***, Mean (± SEM) number of operant responses emitted during signaled cocaine availability (Go) and nonavailability (NoGo) following infusion of either vehicle (Veh) or the nonselective mAChR antagonist scopolamine (Scop, 50 mM) into the LHb. Also shown are the number of responses observed for each rat in these conditions (circles) and, below, mean ± 95% CI estimation plots of the differences between Veh and drug during Go and NoGo periods. Responding during NoGo periods was significantly increased by infusion of Scop into the LHb (two-way repeated-measures ANOVA, Go/NoGo × drug interaction, $F_{(1,8)} = 8.264$, $p = 0.0207$, $^*p = 0.0219$, Sidak's *post hoc*). However, Scop did not significantly affect Go responding for cocaine ($p = 0.71$, Sidak's). ***B***, The M_2-mAChR antagonist AFDX-116 (AFDX, 30 mM) significantly increased NoGo responding without affecting Go responding (two-way repeated-measures ANOVA, Go-NoGo × drug interaction, $F_{(1,8)} = 8.406$, $p = 0.0199$; NoGo responses, $^{**}p = 0.0064$, Go responses, $p = 0.9984$, Sidak's *post hoc*). Below is shown the mean ± 95% CI estimation plot for the effect of AFDX. ***C***, Infusion of the M_1-mAChR antagonist PZP into the LHb did not significantly alter Go/NoGo responding for cocaine (two-way repeated-measures ANOVA, Go-NoGo × drug interaction, $F_{(1,8)} = 0.3536$, $p = 0.685$).

M_2Rs in LHb neurons, our behavioral experiment suggests that endogenous ACh acts via LHb M_2Rs to enable suppression of responding for cocaine in a task in which rats had learned to withhold responses when the drug was not available. Although this implicates LHb ACh and M_2Rs in response inhibition, our experiments do not permit the identification of the presynaptic or postsynaptic sites of M_2R involvement in this model of impulsive behavior. Despite this, response inhibition tasks are used extensively to identify brain circuits underlying impulsive behavior and have translational value in humans (Smith et al., 2014). Therefore, our study suggests that LHb M_2Rs could represent a translational target for therapeutics in the treatment of impulsive behavior, particularly as it relates to addiction.

We previously reported that Oxo-M depolarized ~50% of LHb neurons and hyperpolarized another 10% of these cells (Zapata et al., 2017). Here, we used CCh as an agonist because it exhibits faster pharmacokinetic properties in brain slices. However, we found that CCh initiated inward currents in fewer LHb neurons (31 of 88, 35%), suggesting slightly different pharmacological properties of these agonists. Consistent with this, we observed that some neurons unresponsive to CCh demonstrated robust inward currents with Oxo-M. Therefore, we performed the remainder of the postsynaptic experiments with Oxo-M to characterize mAChRs mediating direct excitation of LHb neurons. We used PZP, considered a relatively selective M_1R antagonist (Doods et al., 1987; Buckley et al., 1989; Valuskova et al., 2018), and AFDX-116, an antagonist with high affinity for M_2Rs (Buckley et al., 1989; Regenold et al., 1989; Lai et al., 1990; Billard et al., 1995). However, additional evidence shows that PZP binds to other mAChRs, including M_4Rs (Bonner, 1989; Hulme et al., 1990; Kashihara et al., 1992; Caulfield and Birdsall, 1998; Dasari and Gulledge, 2011). Similarly, AFDX-116 is reported to have affinity for receptors other than M_2Rs, including M_4Rs (Buckley et al., 1989; Levey et al., 1991; Kashihara et al., 1992; Vilaro et al., 1992a). Because of this, we also examined whether the M_4R PAM, VU10010 (Shirey et al., 2008), would alter the effects of Oxo-M and perhaps reveal the participation of M_4Rs in regulating LHb neuron excitability. However, in contrast to its ability to augment the effects of CCh in the hippocampus, where M_4-mAChRs are known to inhibit glutamate release (Shirey et al., 2008; Thorn et al., 2017), we found that VU10010 had no effect in the LHb. Therefore, this comparative pharmacology shows that AFDX-116 was more efficacious than PZP at reversing inward currents elicited by Oxo-M, and that the effects of Oxo-M are not potentiated by an M_4R PAM. These data, together with the observation that M_2Rs are expressed at moderate to high levels in the LHb (Spencer et al., 1986; Wagner et al., 2016), indicate that the M_2R is the primary mAChR subtype involved in LHb cholinergic signaling.

In contrast to the heterogeneity of effects on somatic excitability, CCh consistently inhibited glutamatergic and GABAergic synaptic inputs to LHb neurons. These LHb output neurons are largely glutamatergic and receive synaptic glutamate input from both extrinsic sources and local recurrent collaterals (Kim and Chang, 2005; Weiss and Veh, 2011). Moreover, there are few intrinsic sources of inhibitory synaptic input to these cells (Brinschwitz et al., 2010; Aizawa et al., 2012; Wagner et al., 2017; Webster et al., 2021), suggesting that inhibitory control of LHb output may arise largely from extrinsic sources. We found that CCh inhibited glutamatergic synaptic sEPSC frequency and amplitude in LHb neurons. As there is evidence for local connectivity among these glutamatergic cells (Kim and Chang, 2005), and we found that some LHb neurons are directly inhibited by CCh, we reasoned that the CCh inhibition of sEPSC amplitude might reflect somatic hyperpolarization, as described for μ-opioid receptors in the LHb (Margolis and Fields, 2016). Consistent with this, blockade of action potential-dependent glutamate release with TTX eliminated the effect of CCh on sEPSC amplitude, but not frequency, suggesting that the reduction in somatic excitability contributed to sEPSC amplitude changes. Moreover, as the decrease in sEPSC frequency and amplitude by CCh was blocked by AFDX-116 (Hulme et al., 1990), it is likely that M_2Rs influence synaptic glutamate release by actions on both somatic excitability and on the axon terminal glutamate release process.

In contrast to its effects on sEPSCs, CCh inhibited sIPSC frequency without changing sIPSC amplitudes. This was also reversed by AFDX-116, but not by PZP, suggesting that M_2Rs on inhibitory axon terminals decrease GABA release probability in LHb neurons, and that M_1Rs are not involved. Additionally, we found that electrically evoked IPSCs, arising from GABAergic axons from undefined projections, were inhibited by M_2Rs, as

were those evoked by specific light activation of ChR2 expressed in VTA afferents to LHb. The input from the VTA represents a major inhibitory afferent that can strongly limit LHb neuron output (Shabel et al., 2014; Barker et al., 2017; Faget et al., 2018), and our study indicates that the inhibition of LHb neurons provided by the VTA may be dampened by endogenous ACh acting at M_2Rs. Beyond our physiological identification of this M_2R modulation, other studies show moderate levels of M_2R expression in the LHb, and M_2R mRNA in VTA projections to LHb (Vilaro et al., 1992b; Wagner et al., 2016). However, as the majority of VTA neurons that project to the mLHb synaptically corelease GABA and glutamate (Root et al., 2014b); and can encode both reward and aversion (Root et al., 2020), future studies should evaluate M_2R involvement on behavioral measures involving this pathway.

Since our study shows that M_2Rs inhibit both glutamatergic and GABAergic synaptic input to LHb neurons, one might ask what the net of effect of this dual modulation might be? To address this, we examined CCh effects on E-I balance by measuring electrically evoked and sEPSCs and sIPSCs in the same LHb neurons. Although CCh significantly decreased both GABA and glutamate release, EPSCs were more strongly inhibited, resulting in a net decrease in the E-I balance. This suggests that the overall effect of M_2R activation is to increase the relative inhibition of LHb neurons. Within the context of the indirect influence the LHb has on midbrain DA neurons via its output to the RMTg (Jhou et al., 2009), these data would predict that activation of LHb M_2Rs might dampen the excitation of the RMTg and hence reduce inhibition of DA neurons to increase their excitability. However, it should also be noted that *in vitro* measurements of E-I balance occur without consideration of the relative activity and contributions of these pathways during behavior. Therefore, E-I balance measured *in vitro* provides a somewhat static estimate of the contribution of M_2Rs to LHb output, and its contributions to behavior and additional *in vivo* studies are required to more fully understand the contributions of mAChR-regulated neurotransmitter release to behavior. To this end, our present studies measuring response inhibition of cocaine seeking provides insight into a behavioral role for M_2Rs. Here, our results show that the withholding of responses for cocaine is impaired during LHb M_2R blockade, suggesting that endogenous ACh and M_2Rs are involved in control of the impulse to seek the drug.

We previously found that, unlike blockade of mAChRs, antagonism of LHb ionotropic glutamatergic receptors, β2-subunit containing nicotinic receptors, D_1 and D_2 DA receptors, and serotonin 5-HT_2 and 5-HT_3 receptors, did not affect inhibition of responding for cocaine (Zapata et al., 2017). Therefore, these behavioral data imply that the inhibition of glutamate release by M2Rs in LHb, as demonstrated in the present study, and these other neurotransmitter systems are not likely involved in control of impulsive cocaine seeking in this model of response inhibition. This suggests a more important role for M_2Rs on inhibitory LHb-projecting neurons.

In conclusion, the results of the present study, and our previous work, suggest that muscarinic cholinergic signaling may have an important influence on LHb function that contributes to the control of impulsive behavior involved in drug seeking, and may also be relevant to substance use, and psychiatric disorders involving impulse control deficits.

References

Aizawa H, Kobayashi M, Tanaka S, Fukai T, Okamoto H (2012) Molecular characterization of the subnuclei in rat habenula. J Comp Neurol 520:4051–4066.

Antoine MW, Langberg T, Schnepel P, Feldman DE (2019) Increased excitation-inhibition ratio stabilizes synapse and circuit excitability in four autism mouse models. Neuron 101:648–661.e644.

Balcita-Pedicino JJ, Omelchenko N, Bell R, Sesack SR (2011) The inhibitory influence of the lateral habenula on midbrain dopamine cells: ultrastructural evidence for indirect mediation via the rostromedial mesopontine tegmental nucleus. J Comp Neurol 519:1143–1164.

Barker DJ, Miranda-Barrientos J, Zhang S, Root DH, Wang HL, Liu B, Calipari ES, Morales M (2017) Lateral preoptic control of the lateral habenula through convergent glutamate and GABA transmission. Cell Rep 21:1757–1769.

Barrot M, Sesack SR, Georges F, Pistis M, Hong S, Jhou TC (2012) Braking dopamine systems: a new GABA master structure for mesolimbic and nigrostriatal functions. J Neurosci 32:14094–14101.

Billard W, Binch H 3rd, Crosby G, McQuade RD (1995) Identification of the primary muscarinic autoreceptor subtype in rat striatum as m2 through a correlation of in vivo microdialysis and in vitro receptor binding data. J Pharmacol Exp Ther 273:273–279.

Bonner TI (1989) The molecular basis of muscarinic receptor diversity. Trends Neurosci 12:148–151.

Brinschwitz K, Dittgen A, Madai VI, Lommel R, Geisler S, Veh RW (2010) Glutamatergic axons from the lateral habenula mainly terminate on GABAergic neurons of the ventral midbrain. Neuroscience 168:463–476.

Buckley NJ, Bonner TI, Buckley CM, Brann MR (1989) Antagonist binding properties of five cloned muscarinic receptors expressed in CHO-K1 cells. Mol Pharmacol 35:469–476.

Caulfield MP, Birdsall NJ (1998) International Union of Pharmacology: XVII. Classification of muscarinic acetylcholine receptors. Pharmacol Rev 50:279–290.

Christoph GR, Leonzio RJ, Wilcox KS (1986) Stimulation of the lateral habenula inhibits dopamine-containing neurons in the substantia nigra and ventral tegmental area of the rat. J Neurosci 6:613–619.

Clements JD, Bekkers JM (1997) Detection of spontaneous synaptic events with an optimally scaled template. Biophys J 73:220–229.

Contestabile A, Fonnum F (1983) Cholinergic and GABAergic forebrain projections to the habenula and nucleus interpeduncularis: surgical and kainic acid lesions. Brain Res 275:287–297.

Dasari S, Gulledge AT (2011) M1 and M4 receptors modulate hippocampal pyramidal neurons. J Neurophysiol 105:779–792.

Doods HN, Mathy MJ, Davidesko D, van Charldorp KJ, de Jonge A, van Zwieten PA (1987) Selectivity of muscarinic antagonists in radioligand and in vivo experiments for the putative M1, M2 and M3 receptors. J Pharmacol Exp Ther 242:257–262.

Ettenberg A, Raven MA, Danluck DA, Necessary BD (1999) Evidence for opponent-process actions of intravenous cocaine. Pharmacol Biochem Behav 64:507–512.

Faget L, Zell V, Souter E, McPherson A, Ressler R, Gutierrez-Reed N, Yoo JH, Dulcis D, Hnasko TS (2018) Opponent control of behavioral reinforcement by inhibitory and excitatory projections from the ventral pallidum. Nat Commun 9:849.

Fibiger HC (1982) The organization and some projections of cholinergic neurons of the mammalian forebrain. Brain Res 257:327–388.

Geisler S, Andres KH, Veh RW (2003) Morphologic and cytochemical criteria for the identification and delineation of individual subnuclei within the lateral habenular complex of the rat. J Comp Neurol 458:78–97.

Hulme EC, Birdsall NJ, Buckley NJ (1990) Muscarinic receptor subtypes. Annu Rev Pharmacol Toxicol 30:633–673.

Jhou TC, Fields HL, Baxter MG, Saper CB, Holland PC (2009) The rostromedial tegmental nucleus (RMTg), a GABAergic afferent to midbrain dopamine neurons, encodes aversive stimuli and inhibits motor responses. Neuron 61:786–800.

Jhou TC, Good CH, Rowley CS, Xu SP, Wang H, Burnham NW, Hoffman AF, Lupica CR, Ikemoto S (2013) Cocaine drives aversive conditioning via delayed activation of dopamine-responsive habenular and midbrain pathways. J Neurosci 33:7501–7512.

Kashihara K, Varga EV, Waite SL, Roeske WR, Yamamura HI (1992) Cloning of the rat M3, M4 and M5 muscarinic acetylcholine receptor

genes by the polymerase chain reaction (PCR) and the pharmacological characterization of the expressed genes. Life Sci 51:955–971.
Kim U, Chang SY (2005) Dendritic morphology, local circuitry, and intrinsic electrophysiology of neurons in the rat medial and lateral habenular nuclei of the epithalamus. J Comp Neurol 483:236–250.
Koob GF, Le Moal M (2008) Addiction and the brain antireward system. Annu Rev Psychol 59:29–53.
Lai J, Bloom JW, Yamamura HI, Roeske WR (1990) Amplification of the rat M2 muscarinic receptor gene by the polymerase chain reaction: functional expression of the M2 muscarinic receptor. Life Sci 47:1001–1013.
Lazaridis I, Tzortzi O, Weglage M, Martin A, Xuan Y, Parent M, Johansson Y, Fuzik J, Furth D, Fenno LE, Ramakrishnan C, Silberberg G, Deisseroth K, Carlen M, Meletis K (2019) A hypothalamus-habenula circuit controls aversion. Mol Psychiatry 24:1351–1368.
Lecca S, Meye FJ, Trusel M, Tchenio A, Harris J, Schwarz MK, Burdakov D, Georges F, Mameli M (2017) Aversive stimuli drive hypothalamus-to-habenula excitation to promote escape behavior. Elife 6:e30697.
Levey AI, Kitt CA, Simonds WF, Price DL, Brann MR (1991) Identification and localization of muscarinic acetylcholine receptor proteins in brain with subtype-specific antibodies. J Neurosci 11:3218–3226.
Li H, Eid M, Pullmann D, Chao YS, Thomas AA, Jhou TC (2021) Entopeduncular nucleus projections to the lateral habenula contribute to cocaine avoidance. J Neurosci 41:298–306.
Margolis EB, Fields HL (2016) Mu opioid receptor actions in the lateral habenula. PLoS One 11:e0159097.
Matsumoto M, Hikosaka O (2007) Lateral habenula as a source of negative reward signals in dopamine neurons. Nature 447:1111–1115.
Meye FJ, Soiza-Reilly M, Smit T, Diana MA, Schwarz MK, Mameli M (2016) Shifted pallidal co-release of GABA and glutamate in habenula drives cocaine withdrawal and relapse. Nat Neurosci 19:1019–1024.
Mori T, Kasem EA, Suzuki-Kouyama E, Cao X, Li X, Kurihara T, Uemura T, Yanagawa T, Tabuchi K (2019) Deficiency of calcium/calmodulin-dependent serine protein kinase disrupts the excitatory-inhibitory balance of synapses by down-regulating GluN2B. Mol Psychiatry 24:1079–1092.
National Research Council (2011) Committee for the Update of the Guide for the Care and Use of Laboratory Animals, Institute for Laboratory Animal Research. Guide for the care and use of laboratory animals, p 220. Washington, DC: National Academies.
Neumann PA, Ishikawa M, Otaka M, Huang YH, Schluter OM, Dong Y (2014) Increased excitability of lateral habenula neurons in adolescent rats following cocaine self-administration. Int J Neuropsychopharmacol 18:pyu109.
Paxinos G, Watson C (2007) The rat brain in stereotaxic coordinates. Amsterdam: Academic/Elsevier.
Regenold W, Araujo DM, Quirion R (1989) Quantitative autoradiographic distribution of [3H]AF-DX 116 muscarinic-M2 receptor binding sites in rat brain. Synapse 4:115–125.
Root DH, Mejias-Aponte CA, Qi J, Morales M (2014a) Role of glutamatergic projections from ventral tegmental area to lateral habenula in aversive conditioning. J Neurosci 34:13906–13910.
Root DH, Mejias-Aponte CA, Zhang S, Wang HL, Hoffman AF, Lupica CR, Morales M (2014b) Single rodent mesohabenular axons release glutamate and GABA. Nat Neurosci 17:1543–1551.
Root DH, Zhang S, Barker DJ, Miranda-Barrientos J, Liu B, Wang HL, Morales M (2018) Selective brain distribution and distinctive synaptic architecture of dual glutamatergic-GABAergic neurons. Cell Rep 23:3465–3479.
Root DH, Barker DJ, Estrin DJ, Miranda-Barrientos JA, Liu B, Zhang S, Wang HL, Vautier F, Ramakrishnan C, Kim YS, Fenno L, Deisseroth K, Morales M (2020) Distinct signaling by ventral tegmental area glutamate, GABA, and combinatorial glutamate-GABA neurons in motivated behavior. Cell Rep 32:108094.
Shabel SJ, Proulx CD, Piriz J, Malinow R (2014) Mood regulation. GABA/glutamate co-release controls habenula output and is modified by antidepressant treatment. Science 345:1494–1498.
Shirey JK, Xiang Z, Orton D, Brady AE, Johnson KA, Williams R, Ayala JE, Rodriguez AL, Wess J, Weaver D, Niswender CM, Conn PJ (2008) An allosteric potentiator of M4 mAChR modulates hippocampal synaptic transmission. Nat Chem Biol 4:42–50.
Smith JL, Mattick RP, Jamadar SD, Iredale JM (2014) Deficits in behavioural inhibition in substance abuse and addiction: a meta-analysis. Drug Alcohol Depend 145:1–33.
Solomon RL (1980) The opponent-process theory of acquired motivation: the costs of pleasure and the benefits of pain. Am Psychol 35:691–712.
Spencer DG Jr, Horvath E, Traber J (1986) Direct autoradiographic determination of M1 and M2 muscarinic acetylcholine receptor distribution in the rat brain: relation to cholinergic nuclei and projections. Brain Res 380:59–68.
Stamatakis AM, Jennings JH, Ung RL, Blair GA, Weinberg RJ, Neve RL, Boyce F, Mattis J, Ramakrishnan C, Deisseroth K, Stuber GD (2013) A unique population of ventral tegmental area neurons inhibits the lateral habenula to promote reward. Neuron 80:1039–1053.
Stamatakis AM, Van Swieten M, Basiri ML, Blair GA, Kantak P, Stuber GD (2016) Lateral hypothalamic area glutamatergic neurons and their projections to the lateral habenula regulate feeding and reward. J Neurosci 36:302–311.
Stopper CM, Tse MT, Montes DR, Wiedman CR, Floresco SB (2014) Overriding phasic dopamine signals redirects action selection during risk/reward decision making. Neuron 84:177–189.
Sutherland RJ (1982) The dorsal diencephalic conduction system: a review of the anatomy and functions of the habenular complex. Neurosci Biobehav Rev 6:1–13.
Thorn CA, Popiolek M, Stark E, Edgerton JR (2017) Effects of M1 and M4 activation on excitatory synaptic transmission in CA1. Hippocampus 27:794–810.
Valuskova P, Farar V, Forczek S, Krizova I, Myslivecek J (2018) Autoradiography of (3)H-pirenzepine and (3)H-AFDX-384 in mouse brain regions: possible insights into M1, M2, and M4 muscarinic receptors distribution. Front Pharmacol 9:124.
Vilaro MT, Wiederhold KH, Palacios JM, Mengod G (1992a) Muscarinic M2-selective ligands also recognize M4 receptors in the rat brain: evidence from combined in situ hybridization and receptor autoradiography. Synapse 11:171–183.
Vilaro MT, Wiederhold KH, Palacios JM, Mengod G (1992b) Muscarinic M2 receptor mRNA expression and receptor binding in cholinergic and non-cholinergic cells in the rat brain: a correlative study using in situ hybridization histochemistry and receptor autoradiography. Neuroscience 47:367–393.
Wagner F, Bernard R, Derst C, French L, Veh RW (2016) Microarray analysis of transcripts with elevated expressions in the rat medial or lateral habenula suggest fast GABAergic excitation in the medial habenula and habenular involvement in the regulation of feeding and energy balance. Brain Struct Funct 221:4663–4689.
Wagner F, Weiss T, Veh RW (2017) Electrophysiological properties of neurons and synapses in the lateral habenular complex (LHb). Pharmacol Biochem Behav 162:38–45.
Webster JF, Vroman R, Balueva K, Wulff P, Sakata S, Wozny C (2020) Disentangling neuronal inhibition and inhibitory pathways in the lateral habenula. Sci Rep 10:8490.
Webster JF, Lecca S, Wozny C (2021) Inhibition within the lateral habenula: implications for affective disorders. Front Behav Neurosci 15:786011.
Weiss T, Veh RW (2011) Morphological and electrophysiological characteristics of neurons within identified subnuclei of the lateral habenula in rat brain slices. Neuroscience 172:74–93.
Woolf NJ, Butcher LL (1986) Cholinergic systems in the rat brain: III. Projections from the pontomesencephalic tegmentum to the thalamus, tectum, basal ganglia, and basal forebrain. Brain Res Bull 16:603–637.
Yang Y, Wang H, Hu J, Hu H (2018) Lateral habenula in the pathophysiology of depression. Curr Opin Neurobiol 48:90–96.
Zapata A, Hwang EK, Lupica CR (2017) Lateral habenula involvement in impulsive cocaine seeking. Neuropsychopharmacology 42:1103–1112.
Zhang L, Hernandez VS, Vazquez-Juarez E, Chay FK, Barrio RA (2016) Thirst is associated with suppression of habenula output and active stress coping: is there a role for a non-canonical vasopressin-glutamate pathway? Front Neural Circuits 10:13.